Journal of Virology

Virology | Full-Length Text

SARS-CoV-2 exploits cellular RAD51 to promote viral propagation: implication of RAD51 inhibitor as a potential drug candidate against COVID-19

Thuy X. Pham,[1] Trang T. X. Huynh,[1] Jiwon Choi,[2] Jae-Bong Lee,[3] Seok-Chan Park,[4] Bumseok Kim,[4] Yun-Sook Lim,[1] Soon B. Hwang[1,5]

AUTHOR AFFILIATIONS See affiliation list on p. 17.

ABSTRACT RAD51 is an important factor involved in the homologous recombination and repair of DNA breaks, which has also been implicated in various virus replication processes. We have previously reported that hepatitis C virus (HCV) exploits cellular RAD51 to promote viral propagation. Since severe acute respiratory syndrome coronavirus 2 (SARS-CoV-2) is also an RNA virus, we interrogated whether SARS-CoV-2 could coopt RAD51 for its propagation. Here, we showed that silencing of RAD51 impaired SARS-CoV-2 propagation. We further demonstrated that RAD51 colocalized with SARS-CoV-2 RNA in Vero E6 cells. Interestingly, RAD51 interacted with SARS-CoV-2 3CL protease. This suggests that RAD51 inhibitors may block SARS-CoV-2 propagation. Hence, we evaluated multiple RAD51 inhibitors as potential drug candidates for coronavirus disease 2019 (COVID-19). Among these, B02, 4′-diisothiocyanostilbene-2,2′-disulfonic acid (DIDS), IBR2, and RI(dl)-2 significantly decreased RNA, protein, and infectious virion levels of Wuhan and variants of SARS-CoV-2. Antiviral activity of DIDS was further confirmed in the Syrian hamster model. Molecular docking model showed that these chemicals interfered with RAD51 through dimerization interface. These data suggest that SARS-CoV-2 exploits host RAD51 to facilitate viral propagation, and hence, RAD51 inhibitor may serve as a putative novel therapeutic agent for the treatment of COVID-19.

IMPORTANCE Viruses are constantly evolving to promote propagation in the host. Here, we show that severe acute respiratory syndrome coronavirus 2 (SARS-CoV-2) utilizes host RAD51 for replication. Silencing of RAD51 impaired SARS-CoV-2 propagation. Viral RNA colocalized with RAD51 in the cytoplasm of SARS-CoV-2-infected cells, suggesting that both viral RNA and RAD51 may form a replication complex. We, therefore, evaluated RAD51 inhibitors as possible therapeutic agents against SARS-CoV-2. Indeed, RAD51 inhibitors exerted antiviral activities against not only Wuhan but also variants of SARS-CoV-2. Molecular docking model shows that RAD51 inhibitors impede SARS-CoV-2 propagation by interfering with dimerization of RAD51. These data suggest that RAD51 may represent a novel host-based drug target for coronavirus disease 2019 treatment.

KEYWORDS SARS-CoV-2, RAD51, COVID-19, RAD51 inhibitor, therapeutic agent

Severe acute respiratory syndrome coronavirus 2 (SARS-CoV-2) is the causative agent of coronavirus disease 2019 (COVID-19). SARS-CoV-2 is a highly transmissible and pathogenic coronavirus that emerged in December 2019 and spread quickly around the world. This virus has infected more than 771 million people worldwide, and COVID-19 has caused over 6.9 million deaths so far (1). SARS-CoV-2 is an RNA virus that belongs to the *Betacoronavirus* genus. Severe acute respiratory syndrome coronavirus, Middle East respiratory syndrome coronavirus, and SARS-CoV-2 can cause severe respiratory failure

Editor Shan-Lu Liu, The Ohio State University, Columbus, Ohio, USA

Address correspondence to Soon B. Hwang, sbhwang@jbnu.ac.kr, or Yun-Sook Lim, yunsolim@hanmail.net.

The authors declare no conflict of interest.

See the funding table on p. 17.

Received 9 November 2023
Accepted 17 November 2023
Published 5 December 2023

and have raised as human respiratory pathogens from animals to humans by zoonotic spillover (2, 3). SARS-CoV-2 preferentially infects the cells of the lower respiratory tract in humans (4). Moreover, SARS-CoV-2 can infect other organs, including lungs, heart, brain, liver, kidneys, and intestines (5–7). SARS-CoV-2 infection can cause arrhythmias, heart and renal failure, gastrointestinal disorders, multi-organ failure, and acute respiratory distress syndrome (8).

Numerous prophylactic SARS-CoV-2 vaccines are currently in use to save hundreds of millions of lives globally (9–12). However, the emergence of the serial variants of concern (VOCs) with their remarkable immune evasion capability demands the most effective strategies to counter SARS-CoV-2 pandemic (13). As of November 2021, the predominant Delta (B.1.617.2) variant has been replaced by the Omicron (B.1.1.529) variant with a higher capacity to escape from protective immunity established through vaccination or infection by earlier VOCs (14, 15). Therefore, differential efficacy and safety of anti-SARS-CoV-2 therapies for the treatment of COVID-19 are required. In these regards, drug repositioning may be an effective strategy for the treatment of COVID-19 (16–18).

RAD51 plays an essential role in DNA damage repair by homologous recombination (HR). RAD51 can bind to both ssDNA and dsDNA with equal affinity during the recombination reaction. RAD51 promotes heteroduplex joint formation, connects the damaged DNA to the undamaged repair template, and mediates homologous pairing to synthesize the DNA across the break (19–21). Importantly, RAD51 has been implicated in various viral propagation processes, including HIV (22–24), human papillomavirus (HPV) (25), hepatitis B virus (HBV) (26), and hepatitis C virus (HCV) (27). In the present study, we showed that knockdown of RAD51 impaired SARS-CoV-2 propagation. RAD51 colocalized with SARS-CoV-2 RNA, suggesting that RAD51 inhibitor might block viral propagation. Indeed, multiple RAD51 inhibitors displayed antiviral activities against SARS-CoV-2 both *in vitro* and *in vivo*. Of note, RAD51 inhibitors displayed broad-spectrum antiviral activity against SARS-CoV-2 variants. We further demonstrated that chemical binding site on RAD51 dimerization interface played a crucial role in anti-SARS-CoV-2 activity. All these data suggest that RAD51 may serve as a druggable host target for SARS-CoV-2 infection, and thus, RAD51 inhibitor may be a potential drug candidate to treat COVID-19.

RESULTS

SARS-CoV-2 exploits RAD51 for its own propagation

Since RAD51 plays an important role in various viral replication processes, we investigated whether RAD51 is also involved in SARS-CoV-2 propagation. To this end, Calu-3 cells were transfected with siRNAs targeting RAD51 and then infected with wild-type and Delta variant of SARS-CoV-2. At 48 h postinfection, the silencing effect of RAD51 on viral protein expression level was determined by immunoblot analysis. Figure 1A shows that RAD51 expression was nearly undetectable in siRNA-transfected cells (lanes 3 and 4 in upper, left panel). As expected, SARS-CoV-2 nucleoprotein level decreased extensively in RAD51-silenced cells. We also showed that SARS-CoV-2 protein level of Delta variant decreased profoundly in RAD51-silenced cells (Fig. 1A, right panel). We verified that the knockdown of RAD51 did not affect the cell viability (data not shown). We further confirmed that silencing of RAD51 significantly decreased virus titer, indicating that RAD51 promoted SARS-CoV-2 propagation (Fig. 1A, bottom panels). To exclude the off-target effect of a RAD51 siRNA, we generated an siRAD51-resistant mutant and cotransfected with siRAD51 into Calu-3 cells. As shown in Fig. 1B, siRAD51-resistant mutant was unable to fully restore the SARS-CoV-2 protein expression level (left panel). However, both SARS-CoV-2 RNA level and infectious virus titer level were significantly recovered by siRAD51-resistant mutant (Fig. 1B, middle and right panels). We also generated the RAD51-siRNA-resistant mutant plasmid and cotransfected with siRAD51 into Calu-3 cells and 293T cells. In fact, Calu-3 cells are widely used for SARS-CoV-2 infection; however, exogenous gene transfection efficiency in Calu-3 cells is very low (data not shown). As shown in Fig. 1C, exogenous expression of the

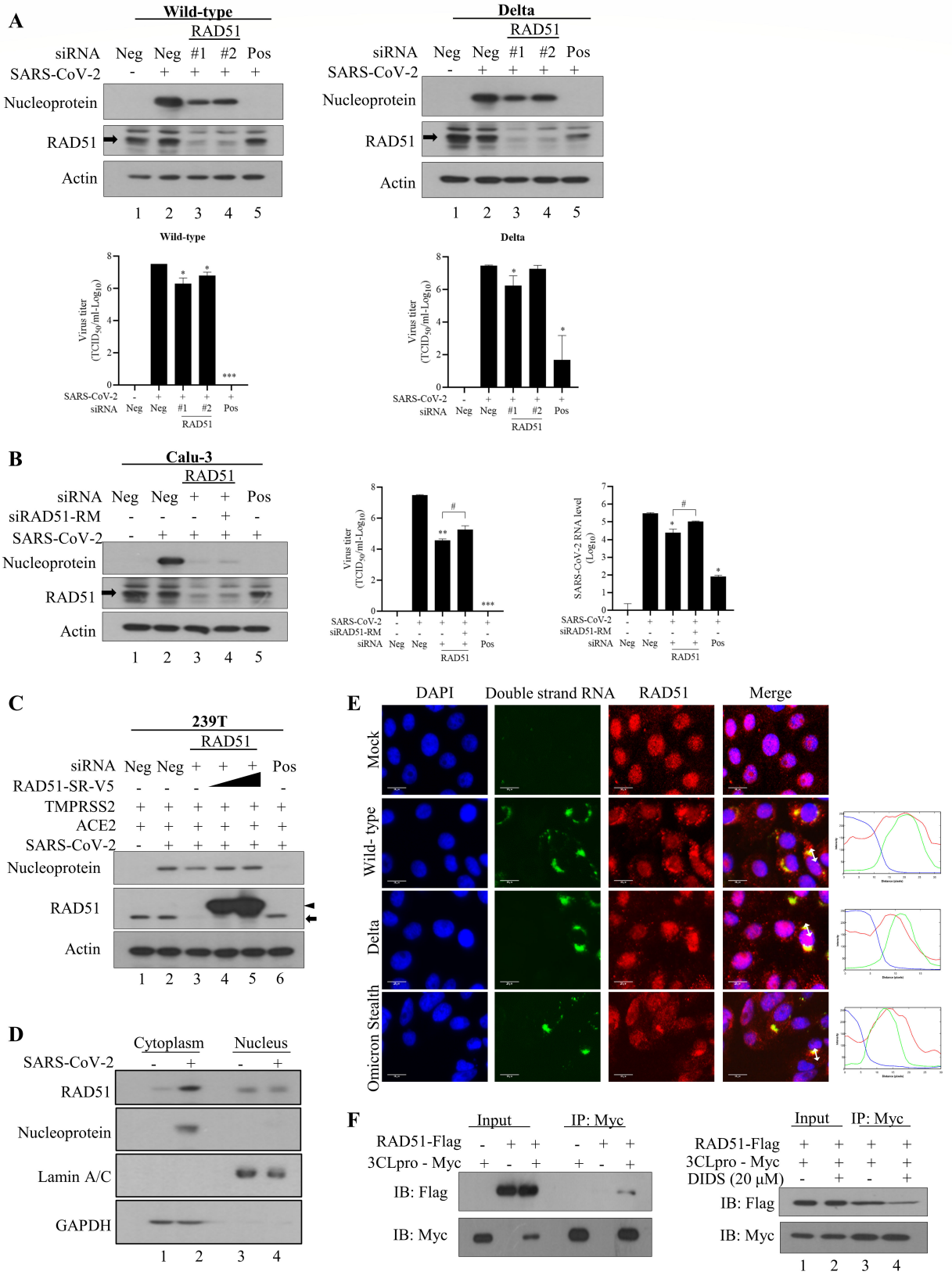

FIG 1 RAD51 is involved in SARS-CoV-2 propagation. (A) siRNA-mediated knockdown of RAD51 expression impairs SARS-CoV-2 propagation in Calu-3 cells. Calu-3 cells were transfected with 20 nM of the indicated siRNAs. At 48 h after transfection, cells were further infected with either wild-type (MOI = 0.1) or Delta variant (MOI = 1) of SARS-CoV-2 for 1 h. At 48 h postinfection, protein expression levels were analyzed by an immunoblot analysis using the indicated antibodies.
(Continued on next page)

FIG 1 (Continued)

50% Tissue culture infectious dose ($TCID_{50}$) values were determined from the SARS-CoV-2-containing supernatant. Wild type, Wuhan strain of SARS-CoV-2; Neg, universal negative siRNA; Pos, positive siRNA targeting the RNA-dependent RNA polymerase (RdRp) of SARS-CoV-2. (B) Calu-3 cells were transfected with 20 nM siRAD51 and 10 nM siRAD51-resistant mutant. Total amounts of siRNA were adjusted by adding negative siRNA. At 48 h after transfection, cells were further infected with wild-type SARS-CoV-2 (MOI = 0.5). At 48 h postinfection, protein expression levels were analyzed by immunoblot analysis using the indicated antibodies, $TCID_{50}$ value was determined from the SARS-CoV-2-containing supernatant, and SARS-CoV-2 RNA level was measured by quantitative real-time PCR. siRNA sequences: RAD51, 5′-GCA GUG AUG UCC UGG AUA A (dT dT)-3′; siRAD51-resistant mutant (siRAD51-RM), 5′-GCA GUG AUG UCU UAG ACA A (dT dT)-3′. For virus titer and SARS-CoV-2 RNA level, one-way ANOVA was calculated to compare the multiple treatments gene-specific siRNA and negative siRNA in SARS-CoV-2-infected cells (*P < 0.05; **P < 0.01; ***P < 0.001). Student's t-test was used for comparing the significant difference between cells cotransfected with siRAD51/siRAD51-RM and cells transfected with siRAD51 (#P < 0.05). (C) 293T cells were cotransfected with 20 nM of the indicated siRNAs, 0.5 µg TMPRSS2 plasmid, 0.5 µg ACE2 plasmid, and 0.5 or 1 µg of V5-tagged RAD51 siRNA-resistant mutant plasmid (RAD51-SR-V5). Total amounts of DNA were adjusted by adding empty vector. At 24 h after transfection, cells were infected with wild-type SARS-CoV-2 (MOI = 0.01). At 24 h postinfection, protein expression levels were analyzed by immunoblot assay. Neg, universal negative siRNA; Pos, positive siRNA targeting the RdRp of SARS-CoV-2. Arrow indicates endogenous RAD51, and arrowhead denotes V5-tagged exogenous RAD51. Data represent averages from triplicate experiments. (D) Vero E6 cells were either mock infected or infected with SARS-CoV-2 (MOI = 0.01) for 1 h and further cultured in fresh media. At 24 h postinfection, both cytosolic and nuclear fractions were prepared, and then protein levels were determined by an immunoblot analysis with the indicated antibodies. (E) Vero E6 cells were either mock infected or infected with wild-type (MOI = 0.01), Delta (MOI = 0.1), and Omicron stealth (MOI = 4) variant of SARS-CoV-2, respectively, for 1 h and further cultured in fresh media. At 24 h postinfection, cells were fixed with 4% paraformaldehyde, and immunofluorescence staining was performed by using either J2 antibody and FITC-conjugated goat anti-mouse IgG to detect dsRNA (green) or anti-Rad51 antibody and TRITC-conjugated donkey anti-rabbit IgG to detect RAD51 (red). Cells were counterstained with 4′,6′-diamidino-2-phenylindole to label nuclei (blue). Plot profile corresponding to the white arrow is traced in the merged panel. Scale bar = 20 µm. (F) (Left panel) 293T cells were cotransfected with Myc-tagged SARS-CoV-2 3CL protease and Flag-tagged RAD51. At 24 h after transfection, total cell lysates were immunoprecipitated with an anti-Myc antibody. Bound protein was detected by an anti-Flag antibody. (Right panel) 293T cells were cotransfected with Myc-tagged SARS-CoV-2 3CL protease and Flag-tagged RAD51. At 24 h after transfection, total cell lysates were mixed with 20 µM DIDS, incubated for 1 h with rotation, and then immunoprecipitated with an anti-Myc antibody. Bound protein was immunoblotted with an anti-Flag antibody.

RAD51-siRNA-resistant mutant restored the SARS-CoV-2 nucleoprotein expression level in 293T cells. These data indicate that RAD51 plays an important role in SARS-CoV-2 propagation. Since SARS-CoV-2 replicates in the cytoplasm and RAD51 is localized in the nucleus, we questioned whether intracellular localization of RAD51 was altered by SARS-CoV-2 infection. For this purpose, both cytosolic and nuclear fractions prepared from either mock- or SARS-CoV-2-infected cells were analyzed by immunoblot using an anti-RAD51 antibody. Figure 1D shows that the RAD51 level in nuclear fraction marginally decreased, whereas the protein level of RAD51 in cytosolic fraction increased markedly in SARS-CoV-2-infected cells compared to mock-infected cells (lane 2 versus lane 1). To further confirm the subcellular re-distribution of RAD51 by SARS-CoV-2 infection, we performed immunofluorescence assay by using an anti-RAD51 antibody and double-strand RNA-specific J2 antibody. As shown in Fig. 1E, RAD51 mainly localized in the nuclei of mock-infected cells. Meanwhile, the protein level of RAD51 barely decreased in the nuclei but prominently accumulated in the cytoplasm of SARS-CoV-2-infected cells. Importantly, RAD51 protein colocalized with replicating viral RNA in cells infected with wild type, Delta, and Omicron stealth of SARS-CoV-2. All these data suggest that SARS-CoV-2 exploits host cellular RAD51 to promote viral propagation. We previously reported that protein interaction between RAD51 and HCV non-structured protein 3 (NS3) is critical for HCV production (27). Since HCV NS3 is a multifunctional protein which displays serine protease and RNA helicase activities, we investigated whether RAD51 also interacted with SARS-CoV-2 3CL protease. SARS-CoV-2 3CL protease is a viral enzyme that plays an essential role in viral replication. To determine protein interaction between RAD51 and SARS-CoV-2 3CL protease, we cotransfected Flag-tagged RAD51 and Myc-tagged SARS-CoV-2 3CL protease plasmid into 293T cells and performed immunoprecipitation assay. Figure 1F showed that RAD51 was coprecipitated with SARS-CoV-2 3CL protease (left panel). Of note, this interaction was impeded by one of the RAD51 inhibitors, 4'-diisothiocyanostilbene-2,2'-disulfonic acid (DIDS; Fig. 1F, lane 4 versus lane 3 in right panel). These data suggest that SARS-CoV-2 may recruit RAD51 via 3CL protease to ensure viral replication. More importantly, RAD51 inhibitor may block SARS-CoV-2 propagation by inhibiting viral RNA synthesis in the replication complex.

RAD51 inhibitors block SARS-CoV-2 propagation

Since RAD51 has been implicated in various viral replication processes and is required for SARS-CoV-2 propagation in the current study, we investigated whether RAD51 inhibitors could block SARS-CoV-2 propagation. For this purpose, we selected six well-known RAD51 inhibitors (B02, RI-1, RI-2, DIDS, RI(dl)-2, and IBR2) to examine their negative role in SARS-CoV-2 propagation. As these chemicals inhibit RAD51 with inhibitory concentration (IC_{50}) values ranging from 0.1 to 45 µM, we decided to use chemical concentrations of 0.1, 1, 5, 10, 20, and 40 µM to evaluate the anti-SARS-CoV-2 activity of each chemical. Next, either Vero E6 cells or Calu-3 cells were mock infected or infected with wild-type SARS-CoV-2 in the absence or presence of the indicated amounts of chemicals. At 24 h (Vero E6) or 48 h (Calu-3) postinfection, both protein and RNA levels of SARS-CoV-2 were determined in RAD51 inhibitor-treated cells. We showed that both protein and RNA levels of SARS-CoV-2 were decreased by B02, DIDS, RI(dl)-2, and IBR2, respectively, in a dose-dependent manner in both Vero E6 and Calu-3 cells (Fig. 2A through E). Meanwhile, both protein and RNA levels of SARS-CoV-2 were not altered by RI-1 or RI-2 (Fig. 2A and B). Of note, SARS-CoV-2 protein levels were completely blocked even in the presence of 10 µM DIDS in Vero E6 cells (Fig. 2C). These data indicate that RAD51 inhibitors truly inhibit SARS-CoV-2 replication, further confirming that RAD51 is required for SARS-CoV-2 propagation.

Evaluation of anti-SARS-CoV-2 activity of RAD51 inhibitors

To determine whether RAD51 inhibitor could exert an anti-SARS-CoV-2 activity, either Vero E6 cells or human pulmonary epithelial Calu-3 cells were infected with wild-type SARS-CoV-2 and then treated with various concentrations of each chemical. We examined the effects of RAD51 inhibitors on the cytopathogenicity of SARS-CoV-2-infected cells. The cytopathic effect (CPE) is prominently observed in SARS-CoV-2-infected African green monkey kidney Vero E6 cells (data not shown). We then evaluated anti-SARS-CoV-2 activity of each chemical. B02, DIDS, and RI(dl)-2 target RAD51-ssDNA and/or RAD51-dsDNA, whereas IBR2, RI-1, and RI-2 target RAD51 protein-protein interaction (28, 29). To this end, Vero E6 cells infected with either mock or SARS-CoV-2 (MOI = 0.01) were treated with the indicated chemicals. At day 2 postinfection, microscopy data showed that SARS-CoV-2-induced CPE was decreased by B02, DIDS, RI(dl)-2, and IBR2, respectively, in a dose-dependent manner (data not shown). Meanwhile, neither RI-1 nor RI-2 altered SARS-CoV-2-induced CPE. Next, we determined 50% inhibitory concentration and 50% cytotoxicity (CC_{50}) based on infectious viral titer and cell viability of each chemical. Water-soluble tetrazolium salt (WST) assay result showed that 40 µM B02 and DIDS displayed no effect on the cell viability of both Vero E6 and Calu-3 cells (Fig. 3A and B). As shown in Fig. 3A, B02 inhibited SARS-CoV-2 propagation with an IC_{50} value of 6.82 µM (95% CI ranging from 0.92 to 39.03) in Vero E6 cells and 5.45 µM (95% CI ranging from 0.84 to 22.59) in Calu-3 cells. Figure 3B shows that IC_{50} value of DIDS is 0.032 µM (95% CI up to 0.25) in Vero E6 cells and 24.95 µM (95% CI ranging from 1.63 to more than 40) in Calu-3 cells. Although DIDS decreased the protein levels and viral titer of SARS-CoV-2 in a dose-dependent manner in Calu-3 cells, the antiviral activity of DIDS in Calu-3 cells was less profound than in Vero E6 cells. This may be due to cell type-specific expression of the host genes involved in SARS-CoV-2 propagation. We further showed that RI(dl)-2 exerted an anti-SARS-CoV-2 activity with IC_{50} value of 8.15 µM (95% CI, 0.04–202.46) in Vero E6 cells and 7.79 µM (95% CI, 0.07–55.76) in Calu-3 cells (Fig. 3C). Lastly, IBR2 exhibited an anti-SARS-CoV-2 activity with IC_{50} value of 9.82 µM (95% CI, 2.84–35.71) in Vero E6 cells and 1.61 µM (95% CI, 0.53–4.51) in Calu-3 cells (Fig. 3D). It is noteworthy that DIDS exerts an exceptionally high anti-SARS-CoV-2 activity in Vero E6 cells with an IC_{50} value of 0.032 µM among six RAD51 inhibitors. Although anti-SARS-CoV-2 activity of DIDS tends to vary in different types of cells, these data suggest that DIDS may be a potential anti-SARS-CoV-2 agent.

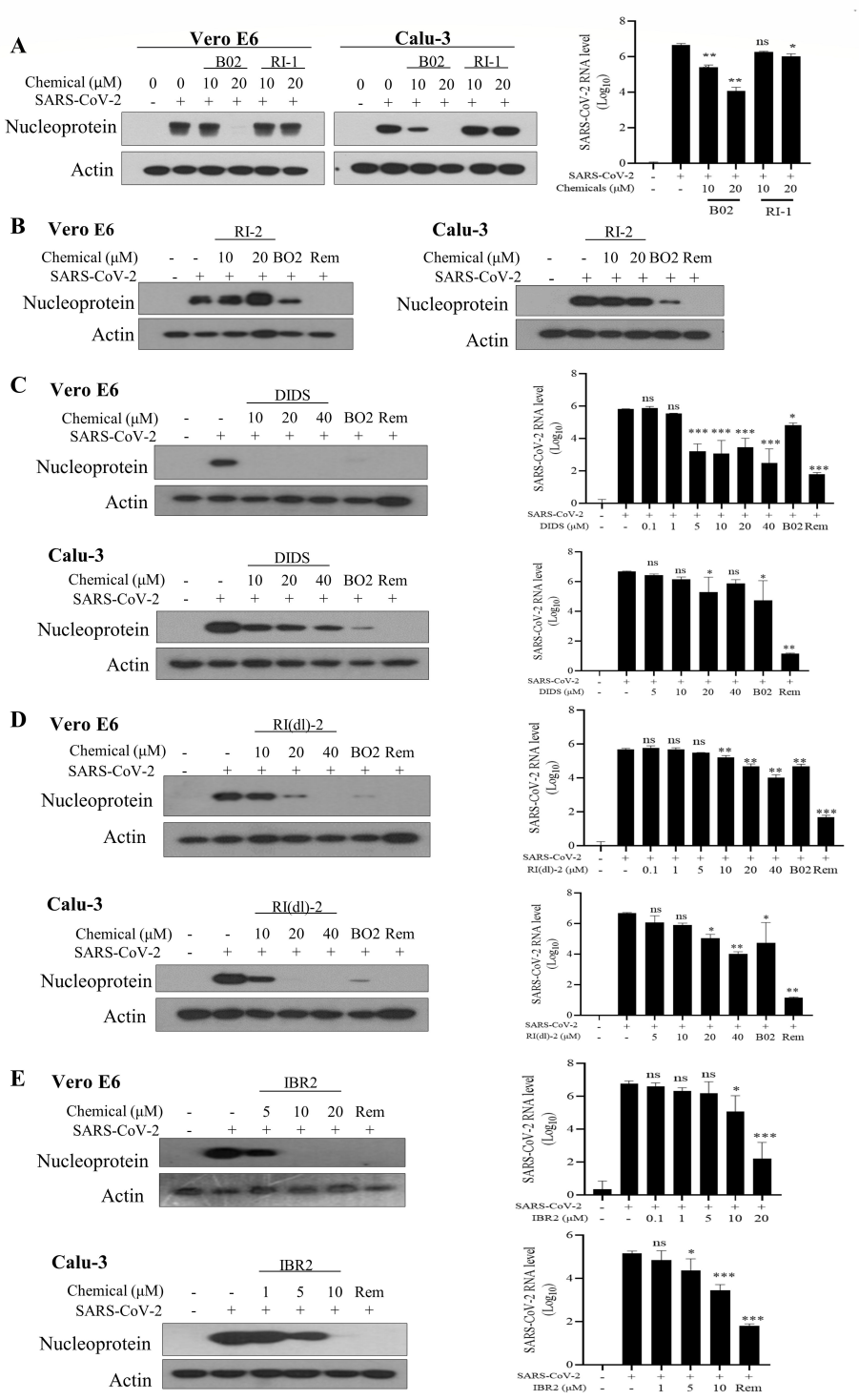

FIG 2 RAD51 inhibitors block SARS-CoV-2 propagation. (A–E) (Left panels) Either Vero E6 cells or Calu-3 cells were mock infected or infected with SARS-CoV-2 (MOI = 0.01 for Vero E6 and MOI = 0.1 for Calu-3) in the absence or presence of the indicated amounts of B02 or RI-1 (A), RI-2 (B), DIDS (C), RI(dl)-2 (D), and IBR2 (E), respectively. At 24 h (Vero E6) or 48 h (Calu-3) postinfection, protein levels of SARS-CoV-2 were determined by an immunoblot assay using the indicated antibodies. (Right panels) At 24 h postinfection, SARS-CoV-2 RNA levels were determined by quantitative real-time PCR. Data represent averages from triplicate experiments. One-way ANOVA was used for comparing the multiple treatments of chemicals and mock-treatment in SARS-CoV-2-infected cells. *P < 0.05; **P < 0.01; ***P < 0.001; ns, not significant. Both B02 (20 μM) and remdesivir (Rem, 5 μM) were used as positive controls.

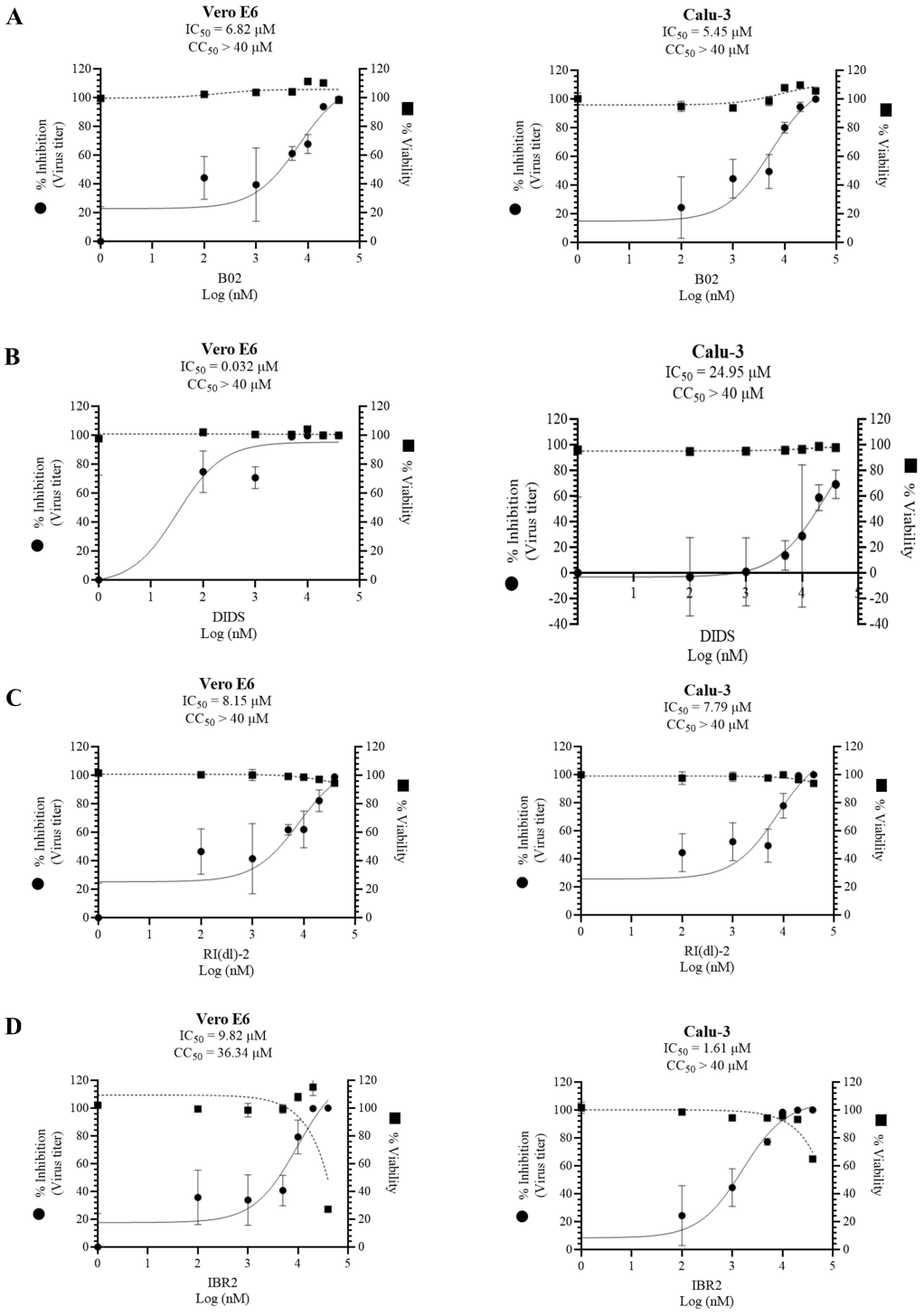

FIG 3 Evaluation of anti-SARS-CoV-2 activity of RAD51 inhibitors. (A–D) Cells were infected with SARS-CoV-2 (MOI = 0.01 for Vero E6; MOI = 0.1 for Calu-3) and either left untreated or treated with B02 (A), DIDS (B), RI(dl)-2 (C), and IBR2 (D), respectively. At 24 h (Vero E6) or 48 h (Calu-3) postinfection, 50% tissue culture infectious dose value was determined from the SARS-CoV-2-containing supernatant. For the "% inhibition" calculation, the normalized relative inhibition values were calculated according to the formula % inhibition = 100 × [1 − (X − mock infected)/(infected untreated − mock infected)], where X is the each given treatment condition. Cell viability was determined by WST assay. Data represent averages from triplicate experiments. Dose-response curves for IC_{50} and CC_{50} values were determined by non-linear regression analysis using the GraphPad Prism 9.

Verification of anti-SARS-CoV-2 activities of RAD51 inhibitors

To verify the antiviral activity of RAD51 inhibitors, Vero E6 cells were either mock infected or infected with wild-type SARS-CoV-2 and treated with either vehicle or 20 µM of the indicated RAD51 inhibitors. SARS-CoV-2 replication was determined by staining cells with double-stranded RNA-specific J2 antibody (30). By using immunofluorescence assay, we showed that SARS-CoV-2 RNA replication was almost abrogated by all of the examined RAD51 inhibitors (Fig. 4A). These data confirmed that B02, DIDS, IBR2, and RI(dl)-2 displayed potent anti-SARS-CoV-2 activities. In February 2022, Omicron variant (B.1.1.529 and BA lineages) has spread globally and outcompeted the most recently recognized Delta variant (B.1.617.2) (31). Since the mutation of SARS-CoV-2 spike protein has led to the genesis of new SARS-CoV-2 variants, we asked whether these RAD51 inhibitors exhibited antiviral activities against SARS-CoV-2 variants. We showed that B02, DIDS, IBR2, and RI(dl)-2 markedly decreased SARS-CoV-2-induced CPE in wild-type, Delta, and Omicron stealth (BA.2 lineage) variants (data not shown). Furthermore, each of these four antiviral compounds profoundly decreased SARS-CoV-2 protein levels in both Vero E6 and Calu-3 cells (Fig. 4B). Collectively, these data suggest that RAD51 inhibitors may have the potential as an effective antiviral against not only known VOCs but also newly emerging SARS-CoV-2 variants. Taken together, these RAD51 inhibitors may represent potential drug candidates to treat COVID-19.

RAD51 inhibitors impede SARS-CoV-2 propagation by interfering with dimerization of RAD51

To explore the structural motif differences between RAD51 and its inhibitors in terms of anti-SARS-CoV-2 activity, we performed molecular docking analysis using the Schrödinger software Glide (32). It has been previously reported that B02 and its derivatives bind within the dimerization interface of a RAD51 filament (33). Therefore, our docking calculations were preferentially performed within the dimerization interface of RAD51 protein using six compounds. Of these RAD51 inhibitors, B02, IBR2, DIDS, and RI(dl)-2 decreased SARS-CoV-2 propagation. Indeed, molecular docking analysis confirmed that these four RAD51 inhibitors showed high affinity at the dimerization interface (Fig. 5A). Grid-based docking results of four ligands in common produced a configuration, in which the aromatic ring of ligands docked into a hydrophobic cavity formed by residues Phe 248 and Met 251, and cation-π interaction with Arg 247 in the dimerization interface of an RAD51 protein (Fig. 5B). We show that anti-SARS-CoV-2 activities of RI-1 and RI-2 are less effective than those of B02, IBR2, DIDS, and RI(dl)-2, which are likely due to a loss of cation-π interaction with Arg 247 (Fig. 5C). Molecular docking studies demonstrate that the four ligands strongly interact with the dimerization interface of RAD51 protein with Glide docking scores of −3.5, −3.9, −4.3, and −4.2 kcal/mol, respectively. These results indicate that the hydrophobic interactions with Phe 248 and Met 251, and cation-π interaction with Arg 247 are critical for ligand binding and that these residues play a key role in ligand potency as well as its binding affinity in the dimerization interface. Taken together, these data further provide the critical importance of structural motif differences among RAD51 inhibitors in anti-SARS-CoV-2 activity, which suggests the better utility of structure-based ligand optimization.

Anti-SARS-CoV-2 activity of RAD51 inhibitor in Syrian hamsters

To further verify the efficacy of RAD51 inhibitor *in vivo*, we chose DIDS because it displayed an exceptionally high anti-SARS-CoV-2 activity, and DIDS also has been clinically used as a drug target for the treatment of hypertension, osteoporosis, and gastrointestinal and renal disorders (34). To this end, we randomly divided Syrian hamsters into mock-infected or SARS-CoV-2-infected group in the absence or presence of DIDS. Animals were intranasally infected with 10^6 of 50% tissue culture infectious dose ($TCID_{50}$) wild-type SARS-CoV-2. Immediately after the virus infection, animals were intraperitoneally injected with 50 mg/kg DIDS. DIDS was treated again on the next day

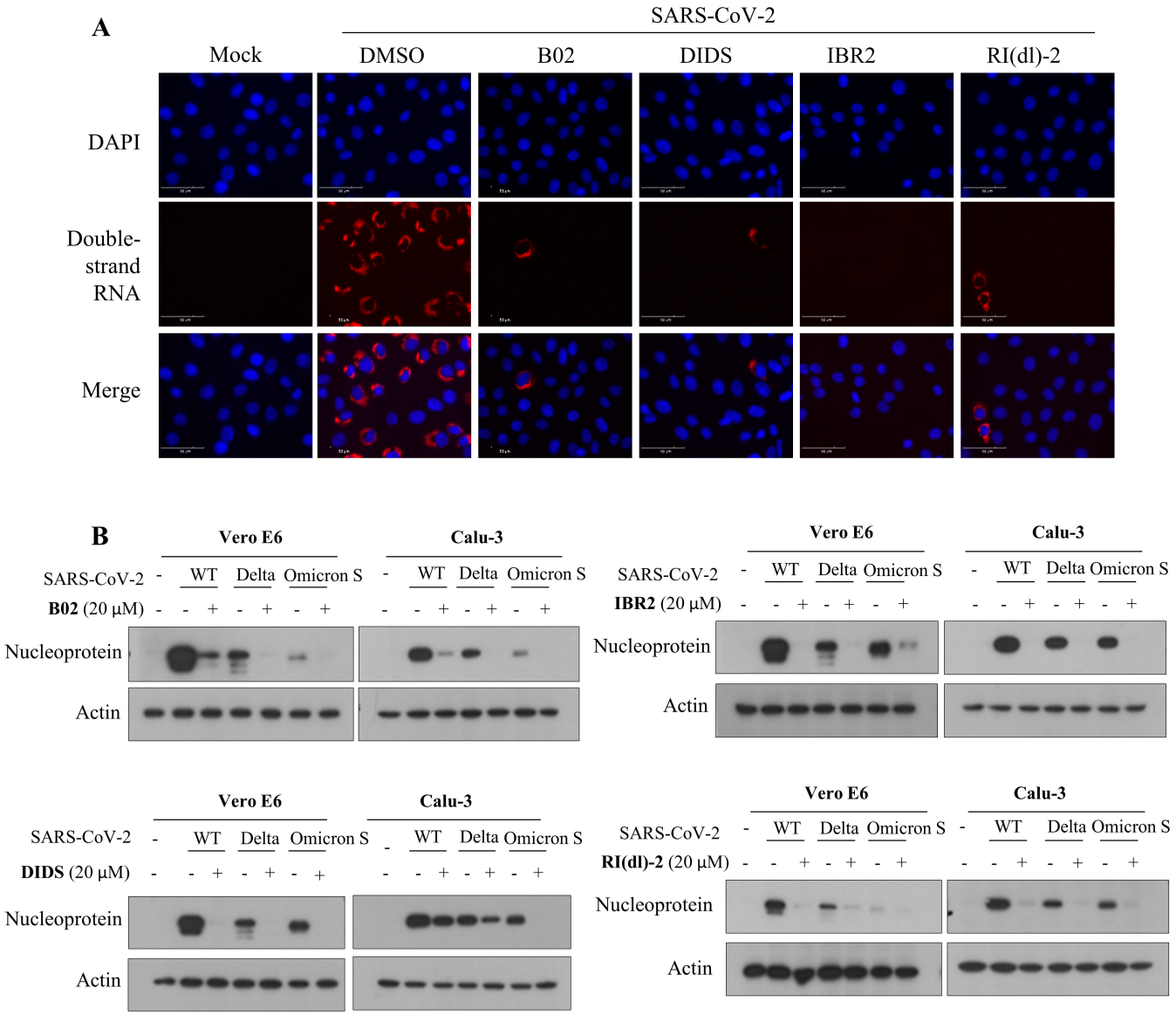

FIG 4 Confirmation of anti-SARS-CoV-2 activity of RAD51 inhibitors. (A) Vero E6 cells were either mock-infected or infected with SARS-CoV-2 (MOI = 0.01) in the absence or presence of 20 µM of the indicated RAD51 inhibitors for 1 h and further cultured in media containing the indicated chemicals. At 24 h post-treatment, cells were fixed in 4% paraformaldehyde, and immunofluorescence staining was performed by using J2 antibody and TRITC-conjugated goat anti-mouse IgG to detect double-stranded RNA (red). Cells were counterstained with 4′,6′-diamidino-2-phenylindole to label nuclei (blue). Scale bar = 50 µm. (B) Vero E6 cells were mock infected or infected with wild-type (WT; MOI = 0.01), Delta (MOI = 0.1), Omicron stealth (MOI = 1) variants of SARS-CoV-2, respectively, for 1 h in the absence or presence of 20 µM of the indicated chemicals. Calu-3 cells were infected with wild-type (MOI = 0.1), Delta (MOI = 1), Omicron stealth (MOI = 2) variants of SARS-CoV-2 and treated as described above. Cells were further cultured in media containing each chemical for 24 h in Vero E6 cells or 48 h in Calu-3 cells. Protein levels were determined by an immunoblot analysis using the indicated antibodies.

(Fig. 6A). At 4 days postinfection, hamsters were euthanized, and both lung and trachea tissues were collected for the determination of viral RNA, immune response genes expression, and virion titer. As shown in Fig. 6B, body weight was not significantly altered by DIDS for 4 days in SARS-CoV-2-infected hamsters. We further demonstrated that SARS-CoV-2 RNA levels in lung tissues noticeably decreased but not significantly after the DIDS treatment (Fig. 6C). Most importantly, infectious virus titer determined by $TCID_{50}$ significantly decreased in lungs of DIDS-treated animals. It is noteworthy that infectious virus titer in trachea also decreased in DIDS-treated hamsters, but the reduction level of virus titer in trachea was less significant than in lungs (Fig. 6D). Since host innate immune

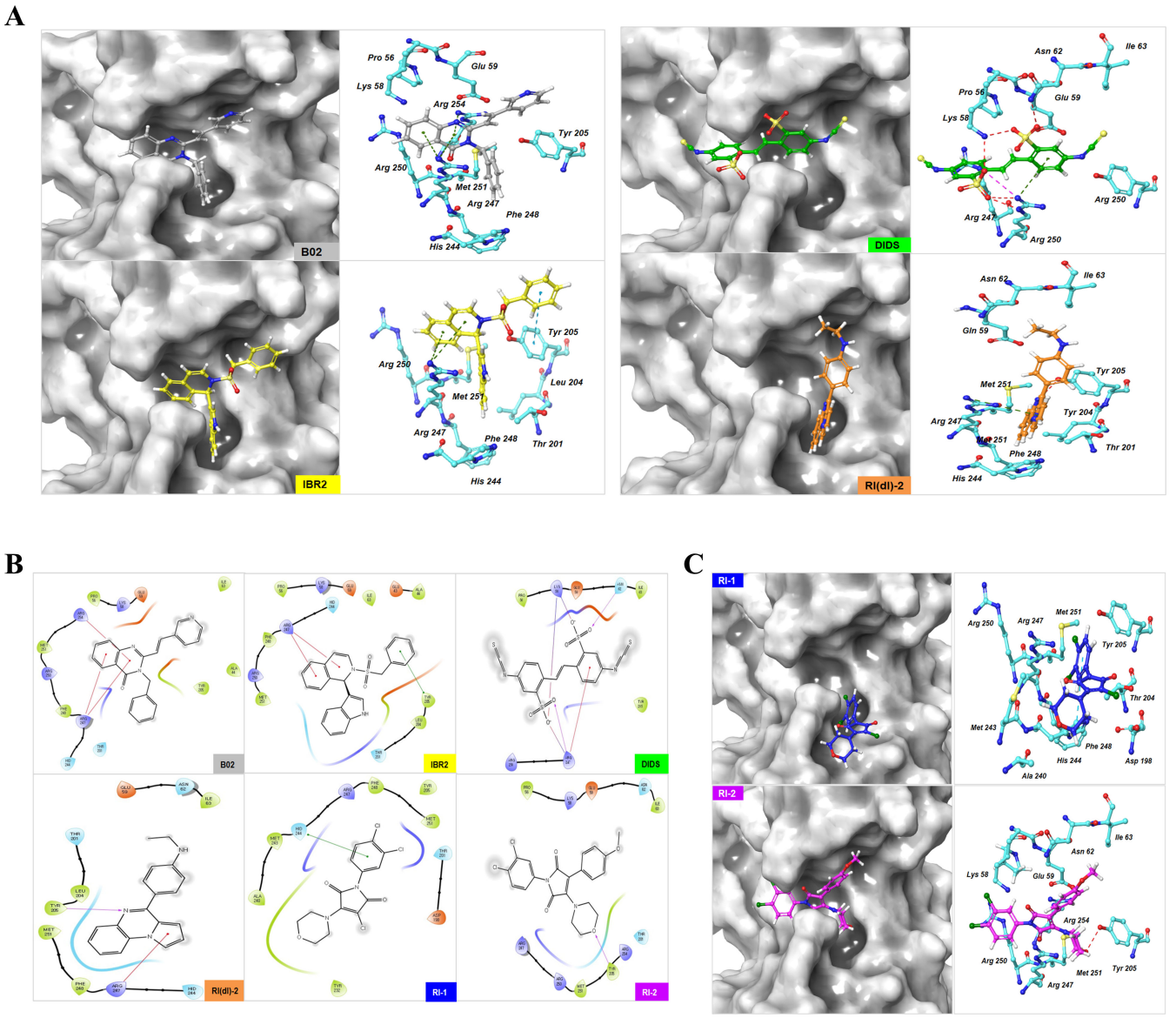

FIG 5 Molecular docking of human RAD51 inhibitors. (A) Binding pose and detailed interactions between RAD51 protein and its inhibitors (B02, IBR2, DIDS, and RI(dl)-2) are shown as a stick model in the dimerization interface. H-bonds are indicated by red-dashed lines. B02, IBR2, DIDS, and RI(dl)-2) are indicated by gray, yellow, green, and orange, respectively. The figures are generated using the PyMoL Molecular Graphics System (Delano Scientific LLC, San Carlos, CA). (B) Ligand diagram reveals interaction between RAD51 protein and its inhibitors (B02, IBR2, DIDS, RI(dl)-2, RI-1, and RI-2). (C) Binding pose of RI-1 and RI-2 to the dimerization interface of RAD51 protein.

response is strictly related to the viral clearance, we investigated the alterations of typical pro-inflammatory cytokines, pro-inflammatory chemokines, and type I interferon (IFN)-related gene expressions in SARS-CoV-2-infected hamsters. As shown in Fig. 6E, the mRNA level of ISG15 in SARS-CoV-2-infected hamsters increased with DIDS treatment, whereas those of IL6, IFN-γ, and CCL5 were decreased by DIDS as compared to mock-treated animals. Interestingly, the mRNA level of TNF-α decreased in SARS-CoV-2-infected hamsters and then restored after treatment with DIDS. These data show that RAD51 inhibitor displays an anti-SARS-CoV-2 activity by modulating host immune response. Collectively, these *in vivo* data further support that DIDS may be a promising novel therapeutic agent for the treatment of COVID-19.

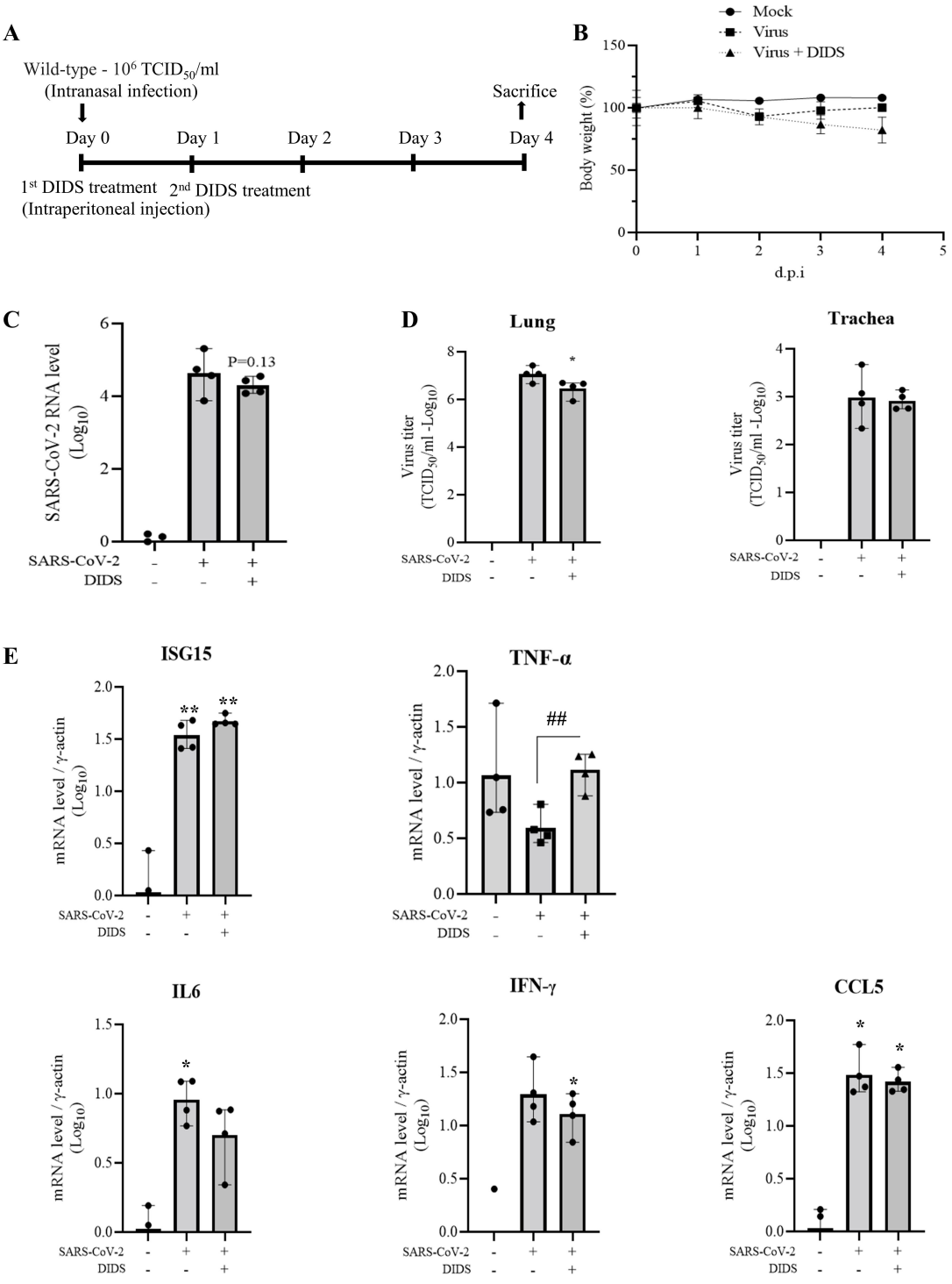

FIG 6 Verification of anti-SARS-CoV-2 activity of DIDS in Syrian hamsters. Syrian hamsters were either mock infected or infected with wild-type SARS-CoV-2 (10^6 $TCID_{50}$) with or without DIDS treatment as illustrated in experimental timeline (A). (B) Body weight progression over time in the indicated group is expressed as the mean ± SD of the percentage over the baseline (day 0 p.i.) weight of each animal (n = 4). (C) At day 4 postinfection, SARS-CoV-2 RNA level in lungs was measured by RT-qPCR. (D) At day 4 postinfection, viral titers ($TCID_{50}$) in the lung (left panel) and trachea (right panel) were determined as described in Materials and Methods. Student's t test was used for comparing the significant difference between mock-treated and DIDS-treated SARS-CoV-2-infected hamsters (*P < 0.05). (E) At day 4 postinfection, mRNA levels of immune response genes in lung tissues were measured by RT-qPCR. One-way ANOVA was calculated to compare the multiple treatments in SARS-CoV-2-infected hamsters and mock-infected hamsters (*P < 0.05, **P < 0.01). Student's t test was used for comparing the significant difference between mock-treated and DIDS-treated SARS-CoV-2-infected hamsters (##P < 0.01).

DISCUSSION

RAD51, an essential factor for HR and DNA repair, has been implicated in various virus propagation processes. RAD51 interacts with HIV-1 integrase to restrict viral integration and replication (22, 23). Both RAD51 and BRCA1 are required for the productive replication of human Papillomavirus 31, suggesting that HR repair system is involved in HPV31 replication (25). RAD51 also regulates HBV infection by maintaining the integrity of the genome and DNA repair (26). We have previously reported that HCV exploits cellular RAD51 to promote viral propagation. RAD51 is co-fractioned with HCV protein on the lipid raft, and hence, we proposed that RAD51 might be a component of the replication complex of HCV (27). Since SARS-CoV-2 is also an RNA virus, we interrogated whether SARS-CoV-2 could coopt RAD51 for its own propagation. In the current study, we showed that silencing of RAD51 expression impaired SARS-CoV-2 propagation in human lung cancer cells. We further showed that RAD51 accumulated in the cytoplasm of SARS-CoV-2-infected cells. It is noteworthy that RAD51 protein is colocalized with viral RNA in SARS-CoV-2-infected Vero E6 cells. It would also be possible that those cells that are heavily infected may have more leaky nuclear membrane, or nuclear import of RAD51 may be impaired in infected cells due to viral cytopathology. These would result in greater amounts of both viral dsRNA and RAD51 in the cytoplasm. Of note, RAD51 inhibitors markedly reduce dsRNA level in SARS-CoV-2-infected cells. Interestingly, we also demonstrated that RAD51 interacted with SARS-CoV-2 3CL protease. These data suggest that SARS-CoV-2 may utilize RAD51 as a component of replication complex to ensure viral replication, and thus, RAD51 may be a potential target to interrupt viral propagation.

SARS-CoV-2 vaccines have been successfully administrated worldwide. However, vaccine breakthrough infections are still common, and immunocompromised patients are not fully protected by current vaccination regimens. Moreover, new VOCs that can evade host immunity are constantly evolving. Therefore, more supportive strategies are needed to effectively control SARS-CoV-2 pandemic. Since RAD51 is involved in SARS-CoV-2 propagation, we selected six well-known RAD51 inhibitors and evaluated their anti-SARS-CoV-2 activities. Among these, B02, DIDS, IBR2, and RI(dl)-2 displayed anti-SARS-CoV-2 activity, respectively, while RI-1 and RI-2 exerted no antiviral activity in Vero E6 and Calu-3 cells. B02, DIDS, and RI(dl)-2 target RAD51-ssDNA or RAD51-dsDNA binding. RI-1, RI-2, and IBR2 inhibit RAD51 filament formation (29). B02 is an inhibitor of human RAD51 with an IC_{50} of 27.4 μM (35). B02 directly binds RAD51 and disrupts RAD51 binding to both ssDNA and dsDNA. B02 specifically inhibits DNA strand exchange and D loop formation activity of human RAD51 (29, 36). DIDS has been used in clinic as an anion transporter inhibitor and chloride channel blocker (34). DIDS directly binds RAD51 and affects RAD51-mediated homologous pairing and strand exchange (37). DIDS inhibits D-loop intermediate structure in a dose-dependent manner with an IC_{50} of 0.9 μM (38). RI(dl)-2 is a cell-permeable pyrroloquinoxaline derivative that specifically inhibits RAD51-mediated D-loop formation (IC_{50} = 11.1 μM) without affecting ssDNA binding. RI(dl)-2 significantly inhibits DSBs-induced cellular HR activity (IC_{50} = 3.0 μM) (29, 39). IBR2 binds to the hydrophobic pocket of RAD51 and inhibits RAD51 oligomerization and filament formation (40). IBR2 also downregulates the protein level and repair activity of RAD51, inhibits the multimerization of RAD51, impairs HR, inhibits cancer cell growth, and induces apoptosis (40, 41). IBR2 disrupts the BRC repeats of BRCA2/RAD51 interaction with IC_{50} of 0.11 μM (40). RI-1 blocks RAD51 protomer-protomer interaction by binding covalently to the surface of RAD51 protein at cysteine 319 residue. Subsequently, RI-1 inhibits RAD51 filament formation and D-loop activity (28, 29, 42). RI-1 blocks RAD51 with IC_{50} ranging from 5 to 30 μM (42). RI-2, an RI-1 analog, is a reversible RAD51 inhibitor (IC_{50} = 44.2 μM), and it competes with RI-1 for binding to RAD51 (28, 29).

In the present study, we demonstrated that B02 significantly reduced SARS-CoV-2 propagation, while RI-1 displayed no anti-SARS-CoV-2 activity. Indeed, a recent study also shows that a human RAD51 inhibitor B02 exhibits antiviral synergy with remdesivir (43). It may be explained by the fact that B02 inhibits RAD51 through ssDNA binding and

dsDNA binding, whereas RI-1 inhibits RAD51 via protein-protein interaction. Similar to B02, DIDS and RI(dl)-2 inhibit RAD51 binding to ssDNA and dsDNA and display anti-SARS-CoV-2 activities. Although RI-1, RI-2, and IBR2 inhibit RAD51 with a similar function, IBR2 remarkably blocks SARS-CoV-2 propagation. We reason that these chemicals have different binding sites on RAD51 since RI-1 and RI-2 bind to RAD51 at cysteine 319 residue (28), whereas IBR2 binds to the hydrophobic pocket of RAD51 (40). Our docking model data further support that both RI-1 and RI-2 show lower binding affinity to the dimerization interface of RAD51 as compared to other RAD51 inhibitors. These results suggest that binding affinity between RAD51 and its inhibitors may play an important role in SARS-CoV-2 propagation. Interestingly, we observed that some RAD51 inhibitors, especially DIDS, displayed anti-SARS-CoV-2 activity with different IC_{50} values either in Vero E6 cells or Calu-3 cells, indicating that there might be cell type-dependent antiviral efficacy of RAD51 inhibitor. This is likely due to the distinctive drug metabolism or cell type-specific gene expression patterns of host factors required for SARS-CoV-2 propagation.

To verify the antiviral activity of RAD51 inhibitor *in vivo*, we selected DIDS and examined its efficacy in Syrian hamsters. In fact, DIDS has been clinically used for the treatment of other diseases (34). Currently, hamsters are widely used for COVID-19 animal studies, although hamster model develops only mild-to-moderate disease (44, 45). We showed that infectious virus titer in lungs significantly decreased in DIDS-treated hamsters. We further found that virus titer in trachea decreased in DIDS-treated hamsters but was less significant than in lungs. Despite the same tendency, SARS-CoV-2 RNA levels decreased but not significantly in lung tissues of DIDS-treated hamsters. We also observed that virus titer level and RNA level were not proportionally decreased by DIDS in SARS-CoV-2-infected animals. It can be explained that the viral load and viral RNA expression level in the lungs and extrapulmonary organs of SARS-CoV-2-infected Syrian hamsters may change dynamically (46). Moreover, it is well established that the particle:pfu ratio for viruses can vary between viral strains and is influenced by the cell type or organism the viral sample has been grown in (47).

An aberrant innate immune response has been reported to contribute to the immunopathology of COVID-19, which is characterized by an impaired type I IFN response and an exacerbated release of proinflammatory cytokines (48–50). Therefore, DIDS may prevent the subsequent cytokine storm by declining IL6 and IFN-γ levels. ISG15 is strongly induced by viral infection and is conjugated to a wide range of viral and host proteins to contribute to the defense against viruses such as influenza, herpes, and Sindbis viruses (51). Likewise, the increase of ISG15 level in DIDS-treated hamsters may represent the antiviral effect of DIDS in SARS-CoV-2-infected animals. In conjunction with the other proinflammatory cytokines, TNF-α can induce localized and systemic inflammatory events that eventually lead to tremendous lung damage and pulmonary edema in COVID-19 lung disease. This demonstrates the importance of TNF-α in the progression of COVID-19 (52–54). However, TNF-α level decreases in SARS-CoV-2-infected Syrian hamsters (46, 55). We speculate that SARS-CoV-2 may regulate immune suppressors to attenuate host immune responses. Hence, DIDS may alleviate disease progression and severity of COVID-19 by modulating TNF-α level. Collectively, our data confirmed that DIDS inhibited viral replication and virion production of SARS-CoV-2 *in vivo*. However, further studies are needed to elucidate the mode of action of DIDS and evaluate antiviral activities of other RAD51 inhibitors. Taken together, our *in vitro* and *in vivo* studies strongly support that RAD51 inhibitor may be a potent agent to block SARS-CoV-2 propagation.

Lastly, we demonstrated that RAD51 inhibitors displayed antiviral activity against SARS-CoV-2 variants, including highly pathogenic Delta and highly transmissible Omicron. These data suggest that RAD51 inhibitors may represent a novel class of broad-spectrum therapeutics for difficult-to-treat COVID-19. In fact, targeting conserved host protein has an advantage in high genetic barrier to viral resistance and has the potential for pangenotypic antiviral activity. We propose that the intracellular

processes are consistent, and thus virus-host interactions would remain in both wild type and variants of SARS-CoV-2. Therefore, this would be a very important finding of the usefulness of host-targeted agent against viruses. Overall, SARS-CoV-2 coopts cellular RAD51 for viral propagation. Molecular docking model further shows that RAD51 inhibitors impede SARS-CoV-2 propagation by interfering with dimerization of RAD51. Thus, RAD51 inhibitor may provide a potential candidate for drug repositioning against COVID-19. Further investigation is required to define the molecular mechanism of the antiviral activity of RAD51 inhibitor.

MATERIALS AND METHODS

Cell culture

All cell lines were grown in Dulbecco's modified Eagle's medium (DMEM) supplemented with 10% fetal bovine serum, 1% penicillin-streptomycin, and 1% non-essential amino acids with 5% CO_2 at 37°C. Cells from passage 3 to 10 were used for experiments, and viral infection was performed when the cell density was ~90%. Calu-3 cells were provided by Korean Cell Line Bank (Seoul, Korea).

Plasmids and DNA transfection

Total cellular RNAs were isolated from Calu-3 cells by using NucleoZOL (Macherey-Nagel). Full-length RAD51, RAD51 mutant and full-length 3CL protease were amplified from cDNA synthesized by using a cDNA Synthesis Kit (Toyobo) according to the manufacturer's instructions. PCR products were inserted into the corresponding enzyme sites of the p3x-FLAG-CMV10 vector (Sigma-Aldrich), pEF6/V5-His B, or pEF6/Myc-His B vector (Invitrogen). All DNA transfections were performed by using a polyethyleneimine reagent (Sigma-Aldrich) as we reported previously (27).

Preparation of infectious SARS-CoV-2

Wild type (Wuhan, NCCP-43331), Delta (NCCP-43405), and Omicron stealth (NCCP-43412) of SARS-CoV-2 were provided by the National Culture Collection for Pathogens, South Korea. Viruses were cultured in Vero E6 cells grown in DMEM supplemented with 2% fetal bovine serum (FBS), 1% penicillin-streptomycin, and HEPES (Invitrogen, USA). Viral titers were determined by the 50% tissue culture infectious dose assay. All experiments were conducted in a biosafety level 3 facility, the Korea Zoonosis Research Institute, Jeonbuk National University.

Chemicals

B02 (SML0346), DIDS (D3514), and RI(dl)-2 (SML1851) were purchased from Sigma-Aldrich (St. Louis, MO, USA); RI-1 (24182) and RI-2 (18397) were from Cayman Chemical (Michigan, USA); IBR2 (HY-103710) was from MedChemExpress, USA.

Water-soluble tetrazolium salt assay

Vero E6 cells seeded on a 96-well plate were treated with the indicated chemicals. At the indicated time points, cell viability was measured using 30 µL of WST (Dail Lab, Korea) as reported previously (56).

$TCID_{50}$

A 50% tissue culture infectious dose assay was performed to determine the infectious titer of cell culture-produced SARS-CoV-2 as described previously (57) with few modifications. Vero E6 cells were seeded on 96-well plates overnight and then infected with 10-fold serial dilutions of the virus-containing supernatants. At 5 days postinfection, virus-infected cells were counted by the presence of CPE in each well under a light microscope.

Quantification of RNA

Total RNA was isolated using NucleoZol (Macherey-Nagel, Germany). cDNA was synthesized by using a cDNA Synthesis Kit (Toyobo) according to the manufacturer's instructions. Quantitative real-time PCR experiments were performed using the CFX Connect real-time system (Bio-Rad Laboratories, Hercules, CA) with following primers: forward, 5′-GTG AAA TGG TCA TGT GTG GCG G-3′ and reverse, 5′-CAA ATG TTA AAA ACA CTA TTA GCA TA-3′ for SARS-CoV-2 polymerase; forward, 5′-TGA CAG CAG TCG GTT GGA GCG-3′ and reverse, 5′-GAC TTC CTG TAA CAA CGC ATC TCA TA-3′ for β-actin.

RNA interference

siRNAs targeting two different regions of RAD51 [#1: 5′-CCA ACG AUG UGA AGA AAU U (dT dT)-3′; #2: 5′-GCA GUG AUG UCC UGG AUA A (dT dT)-3′] (27), siRAD51-resistant mutant, 5′-GCA GUG AUG UCU UAG ACA A (dT dT)-3′, and the universal negative control siRNA were purchased from Bioneer (South Korea). siRNA targeting the RNA-dependent RNA polymerase of the SARS-CoV-2 [5′-GGA AGG AAG UUC UGU UGA A (dT dT)-3′] was used as a positive control (58). siRNA transfection was performed using a Lipofectamine RNAiMax reagent (Invitrogen, Carlsbad, CA) according to the manufacturer's instructions.

Immunoblot analysis

Cells were harvested and lysed in a buffer containing 50 mM Tris HCl (pH 7.5), 150 mM NaCl, 1% NP-40, 1 mM EDTA, 0.25% sodium deoxycholate, 1 mM Na_3VO_4, 1 mM sodium fluoride, 1 mM phenylmethylsulfonyl fluoride (PMSF), 1 mM β-glycerophosphate, and protease inhibitor cocktail (Roche) for 30 min on ice and centrifuged at 12,000 rpm for 10 min at 4°C. The supernatant was collected, and equal amounts of protein were subjected to SDS-PAGE and electrotransferred to a nitrocellulose membrane. The membrane was blocked in Tris-buffered saline with Tween 20 (TBST) buffer [20 mM Tris-HCl (pH 7.6), 150 mM NaCl, and 0.2% Tween 20] containing 5% non-fat dry milk for 1 h and then incubated overnight at 4°C with the indicated antibodies in TBST buffer containing 1% BSA. The SARS-CoV-2 nucleoprotein was detected using an anti-nucleoprotein antibody (Sino Biological, China). Anti-actin and Flag antibodies were purchased from Sigma-Aldrich (USA). c-Myc antibody was from Santa Cruz. An anti-actin antibody was purchased from Sigma-Aldrich (USA). The membrane was then incubated with either horseradish peroxidase-conjugated goat anti-rabbit antibody or goat anti-mouse antibody (Jackson ImmunoResearch Laboratories, West Grove, PA, USA) in TBST buffer for 1 h at room temperature. Proteins were detected using an ECL Kit (Amersham Biosciences).

Immunoprecipitation assay

Cells were cotransfected with the indicated plasmids as described in each experiment. Total amounts of DNA were adjusted by adding an empty vector. At 24 h after transfection, cell lysates were centrifuged at 13,500 rpm at 4°C for 15 min, and then supernatant was incubated at 4°C overnight with the indicated antibody. The samples were further incubated with 30 µL of protein A beads (Sigma-Aldrich) for 1 h. The beads were washed five times in washing buffer, and then bound protein was detected by immunoblot assay.

Molecular docking

The crystal structure of *Homo sapiens* RAD51 post-synaptic complex (PDB code: 7EJE) was prepared as a template for docking simulation, which was performed in Glide software (Maestro, version 13.1, Schrödinger, New York, NY, USA). LigPrep was used to generate 3D ligand structures of six RAD51 inhibitors. To characterize the putative binding sites, the prepared protein structures were submitted to the SiteMap module as implemented in Schrödinger Suite (59, 60). The active grid was generated using the receptor grid application in the Glide module. Docking calculation was performed on a

defined receptor grid using the standard precision mode of Glide (32, 61). Based on the results of individual docking runs for each molecule, at least three of the five docking runs producing similar ligand forms are considered to be consistent. Among these, the ligand forms with the best docking score were selected for further structural analysis.

Immunofluorescence assay

Vero E6 cells were seeded on cover glass overnight and infected with SARS-CoV-2 at an MOI of 0.01. Cells were rinsed in PBS and fixed with 4% paraformaldehyde for 10 min. After two washes in PBS, fixed cells were permeabilized with 0.1% Triton X-100 in PBS for 15 min. Cells were then blocked in 0.5% BSA in PBS for 1 h and incubated with primary antibodies overnight. For labeling, samples were incubated with either mouse monoclonal anti-dsRNA J2 antibody (English & Scientific Consulting, 1/1,000 dilution) or rabbit monoclonal anti-RAD51 (Abcam, 1/300 dilution), rabbit anti-SARS-CoV-2 3CL protease (Cell Signaling Technology, 1/300 dilution) or mouse monoclonal anti-RAD51 (Invitrogen, 1/30 dilution). After three washes in PBS, either cell or tissue sections were incubated with secondary antibodies in PBS for 2 h. For single staining, tetramethylrhodamine isothiocyanate (TRITC)-conjugated goat anti-mouse (Jackson ImmunoResearch Laboratories, 1/1,000 dilution) was used to detect dsRNA. For double staining, RAD51 was detected by TRITC-conjugated donkey anti-rabbit (Jackson ImmunoResearch Laboratories, 1/1,000 dilution), and dsRNA was detected by fluorescein isothiocyanate (FITC)-conjugated goat anti-mouse (Jackson ImmunoResearch Laboratories, 1/1,000 dilution). Or RAD51 was detected by TRITC-conjugated goat anti-mouse (1/1,000 dilution), and 3CL protease was detected by FITC-conjugated goat anti-rabbit (Jackson ImmunoResearch Laboratories, 1/1,000 dilution). Cells were counterstained with 4′,6′-diamidino-2-phenylindole for 10 min to label nuclei. Fluorescence was analyzed by using the Zeiss LSM 700 laser 397 confocal microscopy system (Carl Zeiss, Inc., Thornwood, NY) and CELENA S Digital Imaging System 398 (Logos Biosystems, Inc.).

Nuclear and cytoplasmic fractionation

Nuclear and cytoplasmic fractionation were performed as described previously (27) with few modifications. Vero E6 cells grown on 100 mm dishes were washed twice in PBS, detached by trypsinization, pelleted by centrifugation, washed in PBS, and then resuspended in buffer A [10 mM HEPES (pH 7.6), 10 mM KCl, 0.1 mM EDTA, 1 mM DTT, 0.5 mM PMSF]. After incubation on ice for 15 min, 10% NP40 was added and then vortexed for 10 s at the highest setting. The supernatant was collected by centrifugation at 16,000 × *g* for 5 min at 4°C and saved as a cytoplasmic fraction. The pellet was solubilized in buffer B [20 mM HEPES (pH 7.6), 400 mM NaCl, 1 mM EDTA, 1 mM DTT, 1 mM PMSF]. The solubilized pellet was further centrifuged at 16,000 × *g* for 5 min, and then supernatant was collected and saved as a nuclear fraction.

Hamster challenge study

Six-week-old male Syrian golden hamsters were purchased from Central Laboratory Animal Inc. (Korea). The study protocol details were approved by the Institutional Animal Care and Use Committee, Jeonbuk National University (JBNU 2022-055). Animals were divided into mock-infected group, SARS-CoV-2-infected vehicle-treated group, and SARS-CoV-2-infected DIDS-treated group. Each group consists of four animals ($n = 4$). For challenge studies, hamsters were anesthetized with vaporized isoflurane and inoculated intranasally by pipetting 50 µL of wild-type SARS-CoV-2 (10^6 $TCID_{50}$) dropwise into the nostrils of the hamster. Mock group was intranasally inoculated with saline. DIDS (50 mg/kg, dissolved in saline) was injected intraperitoneally. Hamsters were treated in the same manner daily for the first 2 days. Animals were weighed and assessed twice daily for disease progression. For trachea and lung tissue collection, all hamsters were euthanized at day 4 postinfection. All procedures were performed on anesthetized animals.

Statistical analysis

Data are presented as the means ± standard deviations. Statistical analysis was performed by Student's *t* test for two treatments and one-way analysis of variance for multiple treatments. Dunnett's test was used as a post hoc test. All statistical analyses were performed using IBM SPSS statistic v22 (IBM). Half-maximal effective (IC_{50}) cytotoxic (CC_{50}) concentrations of the compounds were estimated by non-linear regression analysis using the GraphPad Prism v9 (GraphPad Software, San Diego, CA, USA). All graphs were drawn using GraphPad Prism. The asterisks or sharp in the figures indicate significant differences (*$P < 0.05$; **$P < 0.01$; ***$P < 0.001$; ns, not significant).

ACKNOWLEDGMENTS

This work was supported by the National Research Foundation of Korea (NRF) grant funded by the Korea government (MSIT) (2021R1A2C2003275 for S.B.H.). This work was also supported by the National Research Foundation of Korea (NRF) grant funded by the Korea government (MSIT) (2022R1A2B5B01001390 for Y.S.L.).

All authors have given approval to the final version of the manuscript. T.X.P. performed experiments, analyzed data, and wrote the manuscript. T.T.X.H. performed experiments. J.C., J.L., S.C.P., and B.K. provided reagents and expertise. Y.S.L. and S.B.H. designed experiments and secured funding. S.B.H. supervised the study and wrote the manuscript.

AUTHOR AFFILIATIONS

[1]Laboratory of RNA Viral Diseases, Korea Zoonosis Research Institute, Jeonbuk National University, Iksan, South Korea
[2]College of Pharmacy, Dongduk Women's University, Seoul, South Korea
[3]Korea Zoonosis Research Institute, Jeonbuk National University, Iksan, South Korea
[4]Laboratory of Veterinary Pathology, College of Veterinary Medicine, Jeonbuk National University, Iksan, South Korea
[5]Ilsong Institute of Life Science, Hallym University, Seoul, South Korea

AUTHOR ORCIDs

Thuy X. Pham http://orcid.org/0000-0002-9796-8493
Yun-Sook Lim http://orcid.org/0000-0003-2659-6669
Soon B. Hwang http://orcid.org/0000-0002-8718-1793

FUNDING

Funder	Grant(s)	Author(s)
Ministry of Science and ICT, South Korea (MSIT)	2021R1A2C2003275	Soon B. Hwang
Ministry of Science and ICT, South Korea (MSIT)	2022R1A2B5B01001390	Yun-Sook Lim

REFERENCES

1. WHO. 2023. WHO coronavirus disease (COVID-19) dashboard
2. Tang D, Comish P, Kang R, Hobman TC. 2020. The hallmarks of COVID-19 disease. PLoS Pathog 16:e1008536. https://doi.org/10.1371/journal.ppat.1008536
3. Morens DM, Folkers GK, Fauci AS. 2008. Emerging infections: a perpetual challenge. Lancet Infect Dis 8:710–719. https://doi.org/10.1016/S1473-3099(08)70256-1
4. Zou L, Ruan F, Huang M, Liang L, Huang H, Hong Z, Yu J, Kang M, Song Y, Xia J, Guo Q, Song T, He J, Yen H-L, Peiris M, Wu J. 2020. SARS-CoV-2 viral load in upper respiratory specimens of infected patients. N Engl J Med 382:1177–1179. https://doi.org/10.1056/NEJMc2001737
5. Lamers MM, Beumer J, van der Vaart J, Knoops K, Puschhof J, Breugem TI, Ravelli RBG, Paul van Schayck J, Mykytyn AZ, Duimel HQ, van Donselaar E, Riesebosch S, Kuijpers HJH, Schipper D, van de Wetering WJ, de Graaf M, Koopmans M, Cuppen E, Peters PJ, Haagmans BL, Clevers H. 2020. SARS-CoV-2 productively infects human gut enterocytes. Science 369:50–54. https://doi.org/10.1126/science.abc1669
6. Puelles VG, Lütgehetmann M, Lindenmeyer MT, Sperhake JP, Wong MN, Allweiss L, Chilla S, Heinemann A, Wanner N, Liu S, Braun F, Lu S, Pfefferle S, Schröder AS, Edler C, Gross O, Glatzel M, Wichmann D, Wiech T, Kluge S, Pueschel K, Aepfelbacher M, Huber TB. 2020. Multiorgan and renal tropism of SARS-CoV-2. N Engl J Med 383:590–592. https://doi.org/10.1056/NEJMc2011400

7. Lin L, Jiang X, Zhang Z, Huang S, Zhang Z, Fang Z, Gu Z, Gao L, Shi H, Mai L, Liu Y, Lin X, Lai R, Yan Z, Li X, Shan H. 2020. Gastrointestinal symptoms of 95 cases with SARS-CoV-2 infection. Gut 69:997–1001. https://doi.org/10.1136/gutjnl-2020-321013
8. Gupta A, Madhavan MV, Sehgal K, Nair N, Mahajan S, Sehrawat TS, Bikdeli B, Ahluwalia N, Ausiello JC, Wan EY, et al. 2020. Extrapulmonary manifestations of COVID-19. Nat Med 26:1017–1032. https://doi.org/10.1038/s41591-020-0968-3
9. Krammer F. 2020. SARS-CoV-2 vaccines in development. Nature 586:516–527. https://doi.org/10.1038/s41586-020-2798-3
10. Polack FP, Thomas SJ, Kitchin N, Absalon J, Gurtman A, Lockhart S, Perez JL, Pérez Marc G, Moreira ED, Zerbini C, et al. 2020. Safety and efficacy of the BNT162b2 mRNA Covid-19 vaccine. N Engl J Med 383:2603–2615. https://doi.org/10.1056/NEJMoa2034577
11. Baden LR, El Sahly HM, Essink B, Kotloff K, Frey S, Novak R, Diemert D, Spector SA, Rouphael N, Creech CB, et al. 2021. Efficacy and safety of the mRNA-1273 SARS-CoV-2 vaccine. N Engl J Med 384:403–416. https://doi.org/10.1056/NEJMoa2035389
12. Voysey M, Clemens SAC, Madhi SA, Weckx LY, Folegatti PM, Aley PK, Angus B, Baillie VL, Barnabas SL, Bhorat QE, et al. 2021. Safety and efficacy of the ChAdOx1 nCoV-19 vaccine (AZD1222) against SARS-CoV-2: an interim analysis of four randomised controlled trials in Brazil, South Africa, and the UK. Lancet 397:99–111. https://doi.org/10.1016/S0140-6736(20)32661-1
13. Rosenke K, Okumura A, Lewis MC, Feldmann F, Meade-White K, Bohler WF, Griffin A, Rosenke R, Shaia C, Jarvis MA, Feldmann H. 2022. Molnupiravir inhibits SARS-CoV-2 variants including Omicron in the hamster model. JCI insight 7:e160108. https://doi.org/10.1172/jci.insight.160108
14. Karim SSA, Karim QA. 2021. Omicron SARS-CoV-2 variant: a new chapter in the COVID-19 pandemic. Lancet 398:2126–2128. https://doi.org/10.1016/S0140-6736(21)02758-6
15. Cao Y, Wang J, Jian F, Xiao T, Song W, Yisimayi A, Huang W, Li Q, Wang P, An R, et al. 2022. Omicron escapes the majority of existing SARS-CoV-2 neutralizing antibodies. Nature 602:657–663. https://doi.org/10.1038/s41586-021-04385-3
16. Guy RK, DiPaola RS, Romanelli F, Dutch RE. 2020. Rapid repurposing of drugs for COVID-19. Science 368:829–830. https://doi.org/10.1126/science.abb9332
17. Law GL, Tisoncik-Go J, Korth MJ, Katze MG. 2013. Drug repurposing: a better approach for infectious disease drug discovery?Curr Opin Immunol 25:588–592. https://doi.org/10.1016/j.coi.2013.08.004
18. Touret F, Gilles M, Barral K, Nougairède A, van Helden J, Decroly E, de Lamballerie X, Coutard B. 2020. *In vitro* screening of a FDA approved chemical library reveals potential inhibitors of SARS-CoV-2 replication. Sci Rep 10:13093. https://doi.org/10.1038/s41598-020-70143-6
19. Gupta RC, Bazemore LR, Golub EI, Radding CM. 1997. Activities of human recombination protein RAD51. Proc Natl Acad Sci U S A 94:463–468. https://doi.org/10.1073/pnas.94.2.463
20. Baumann P, West SC. 1998. Role of the human RAD51 protein in homologous recombination and double-stranded-break repair. Trends Biochem Sci 23:247–251. https://doi.org/10.1016/S0968--0004(98)01232-8
21. Budke B, Lv W, Kozikowski AP, Connell PP. 2016. Recent developments using small molecules to target RAD51: how to best modulate RAD51 for anticancer therapy? ChemMedChem 11:2468–2473. https://doi.org/10.1002/cmdc.201600426
22. Thierry S, Benleulmi MS, Sinzelle L, Thierry E, Calmels C, Chaignepain S, Waffo-Teguo P, Merillon J-M, Budke B, Pasquet J-M, Litvak S, Ciuffi A, Sung P, Connell P, Hauber I, Hauber J, Andreola M-L, Delelis O, Parissi V. 2015. Dual and opposite effects of hRAD51 chemical modulation on HIV-1 integration. Chem Biol 22:712–723. https://doi.org/10.1016/j.chembiol.2015.04.020
23. Cosnefroy O, Tocco A, Lesbats P, Thierry S, Calmels C, Wiktorowicz T, Reigadas S, Kwon Y, De Cian A, Desfarges S, Bonot P, San Filippo J, Litvak S, Le Cam E, Rethwilm A, Fleury H, Connell PP, Sung P, Delelis O, Andréola ML, Parissi V. 2012. Stimulation of the human RAD51 nucleofilament restricts HIV-1 integration *in vitro* and in infected cells. J Virol 86:513–526. https://doi.org/10.1128/JVI.05425-11
24. Kaminski R, Wollebo HS, Datta PK, White MK, Amini S, Khalili K. 2014. Interplay of RAD51 with NF-κB pathway stimulates expression of HIV-1. PLoS One 9:e98304. https://doi.org/10.1371/journal.pone.0098304
25. Chappell WH, Gautam D, Ok ST, Johnson BA, Anacker DC, Moody CA, Ross SR. 2016. Homologous recombination repair factors RAD51 and BRCA1 are necessary for productive replication of human papillomavirus 31. J Virol 90:2639–2652. https://doi.org/10.1128/JVI.02495-15
26. Pasaje CFA, Kim J, Park B, Cheong HS, Bae JS, Park T, Lee J, Kim Y, Lee H, Koh I, Kim YJ, Shin HD. 2011. Lack of association of RAD51 genetic variations with hepatitis B virus clearance and occurrence of hepatocellular carcinoma in a Korean population. J Med Virol 83:1892–1899. https://doi.org/10.1002/jmv.22122
27. Son K, Nguyen TTT, Choi J-W, Pham LV, Luong TTD, Lim Y-S, Hwang SB. 2017. RAD51 interacts with non-structural 3 protein of hepatitis C virus and regulates viral production. Front Microbiol 8:1249. https://doi.org/10.3389/fmicb.2017.01249
28. Budke B, Kalin JH, Pawlowski M, Zelivianskaia AS, Wu M, Kozikowski AP, Connell PP. 2013. An optimized RAD51 inhibitor that disrupts homologous recombination without requiring Michael acceptor reactivity. J Med Chem 56:254–263. https://doi.org/10.1021/jm301565b
29. Grundy MK, Buckanovich RJ, Bernstein KA. 2020. Regulation and pharmacological targeting of RAD51 in cancer. NAR Cancer 2. https://doi.org/10.1093/narcan/zcaa024
30. Pape C, Remme R, Wolny A, Olberg S, Wolf S, Cerrone L, Cortese M, Klaus S, Lucic B, Ullrich S. 2021. Microscopy - based assay for semi - quantitative detection of SARS - CoV - 2 specific antibodies in human sera: a semi - quantitative, high throughput, microscopy - based assay expands existing approaches to measure SARS - CoV - 2 specific antibody levels in human sera. Bioessays 43:2000257. https://doi.org/10.1002/bies.202000257
31. Kimura I, Yamasoba D, Tamura T, Nao N, Suzuki T, Oda Y, Mitoma S, Ito J, Nasser H, Zahradnik J, et al. 2022. Virological characteristics of the SARS-CoV-2 Omicron BA.2 subvariants, including BA.4 and BA.5. Cell 185:3992–4007. https://doi.org/10.1016/j.cell.2022.09.018
32. Friesner RA, Banks JL, Murphy RB, Halgren TA, Klicic JJ, Mainz DT, Repasky MP, Knoll EH, Shelley M, Perry JK, Shaw DE, Francis P, Shenkin PS. 2004. Glide: a new approach for rapid, accurate docking and scoring. 1. Method and assessment of docking accuracy. J Med Chem 47:1739–1749. https://doi.org/10.1021/jm0306430
33. Shkundina IS, Gall AA, Dick A, Cocklin S, Mazin AV. 2021. New RAD51 inhibitors to target homologous recombination in human cells. Genes 12:920. https://doi.org/10.3390/genes12060920
34. Wulff H. 2008. New light on the "old" chloride channel blocker DIDS. ACS Chem Biol 3:399–401. https://doi.org/10.1021/cb800140m
35. Huang F, Motlekar NA, Burgwin CM, Napper AD, Diamond SL, Mazin AV. 2011. Identification of specific inhibitors of human RAD51 recombinase using high-throughput screening. ACS Chem Biol 6:628–635. https://doi.org/10.1021/cb100428c
36. Huang F, Mazina OM, Zentner IJ, Cocklin S, Mazin AV. 2012. Inhibition of homologous recombination in human cells by targeting RAD51 recombinase. J Med Chem 55:3011–3020. https://doi.org/10.1021/jm201173g
37. Ishida T, Takizawa Y, Kainuma T, Inoue J, Mikawa T, Shibata T, Suzuki H, Tashiro S, Kurumizaka H. 2009. DIDS, a chemical compound that inhibits RAD51-mediated homologous pairing and strand exchange. Nucleic Acids Res 37:3367–3376. https://doi.org/10.1093/nar/gkp200
38. Velic D, Demeyer A, Peterlini T, Benhelli-Mokrani H, Mathé-Allainmat M, Masson J-Y, Fleury F. 2021. Molecular determinant of DIDS analogs targeting RAD51 activity. Molecules 26:5460. https://doi.org/10.3390/molecules26185460
39. Lv W, Budke B, Pawlowski M, Connell PP, Kozikowski AP. 2016. Development of small molecules that specifically inhibit the D-loop activity of RAD51. J Med Chem 59:4511–4525. https://doi.org/10.1021/acs.jmedchem.5b01762
40. Zhu J, Zhou L, Wu G, Konig H, Lin X, Li G, Qiu X-L, Chen C-F, Hu C-M, Goldblatt E, Bhatia R, Chamberlin AR, Chen P-L, Lee W-H. 2013. A novel small molecule RAD51 inactivator overcomes imatinib - resistance in chronic myeloid leukaemia. EMBO Mol Med 5:353–365. https://doi.org/10.1002/emmm.201201760
41. Ferguson PJ, Vincent MD, Koropatnick J. 2018. Synergistic antiproliferative activity of the RAD51 inhibitor IBR2 with inhibitors of receptor

tyrosine kinases and microtubule protein. J Pharmacol Exp Ther 364:46–54. https://doi.org/10.1124/jpet.117.241661
42. Budke B, Logan HL, Kalin JH, Zelivianskaia AS, Cameron McGuire W, Miller LL, Stark JM, Kozikowski AP, Bishop DK, Connell PP. 2012. RI-1: a chemical inhibitor of RAD51 that disrupts homologous recombination in human cells. Nucleic Acids Res 40:7347–7357. https://doi.org/10.1093/nar/gks353
43. Biering SB, Van Dis E, Wehri E, Yamashiro LH, Nguyenla X, Dugast-Darzacq C, Graham TGW, Stroumza JR, Golovkine GR, Roberts AW, Fines DM, Spradlin JN, Ward CC, Bajaj T, Dovala D, Schulze-Gamen U, Bajaj R, Fox DM, Ott M, Murthy N, Nomura DK, Schaletzky J, Stanley SA. 2021. Screening a library of FDA-approved and bioactive compounds for antiviral activity against SARS-CoV-2. ACS Infect Dis 7:2337–2351. https://doi.org/10.1021/acsinfecdis.1c00017
44. Imai M, Iwatsuki-Horimoto K, Hatta M, Loeber S, Halfmann PJ, Nakajima N, Watanabe T, Ujie M, Takahashi K, Ito M, et al. 2020. Syrian hamsters as a small animal model for SARS-CoV-2 infection and countermeasure development. Proc Natl Acad Sci U S A 117:16587–16595. https://doi.org/10.1073/pnas.2009799117
45. Muñoz-Fontela C, Dowling WE, Funnell SGP, Gsell P-S, Riveros-Balta AX, Albrecht RA, Andersen H, Baric RS, Carroll MW, Cavaleri M, et al. 2020. Animal models for COVID-19. Nature 586:509–515. https://doi.org/10.1038/s41586-020-2787-6
46. Yang S-J, Wei T-C, Hsu C-H, Ho S-N, Lai C-Y, Huang S-F, Chen Y-Y, Liu S-J, Yu G-Y, Dou H-Y. 2021. Characterization of virus replication, pathogenesis, and cytokine responses in Syrian hamsters inoculated with SARS-CoV-2. J Inflamm Res 14:3781–3795. https://doi.org/10.2147/JIR.S323026
47. McCormick W, Mermel LA. 2021. The basic reproductive number and particle-to-plaque ratio: comparison of these two parameters of viral infectivity. Virol J 18:1–4. https://doi.org/10.1186/s12985-021-01566-4
48. Zhang Q, Bastard P, Liu Z, Le Pen J, Moncada-Velez M, Chen J, Ogishi M, Sabli IKD, Hodeib S, Korol C, et al. 2020. Inborn errors of type I IFN immunity in patients with life-threatening COVID-19. Science 370:eabd4570. https://doi.org/10.1126/science.abd4570
49. Blanco-Melo D, Nilsson-Payant BE, Liu W-C, Uhl S, Hoagland D, Møller R, Jordan TX, Oishi K, Panis M, Sachs D, Wang TT, Schwartz RE, Lim JK, Albrecht RA, tenOever BR. 2020. Imbalanced host response to SARS-CoV-2 drives development of COVID-19. Cell 181:1036–1045. https://doi.org/10.1016/j.cell.2020.04.026
50. Karki R, Sharma BR, Tuladhar S, Williams EP, Zalduondo L, Samir P, Zheng M, Sundaram B, Banoth B, Malireddi RKS, Schreiner P, Neale G, Vogel P, Webby R, Jonsson CB, Kanneganti T-D. 2021. Synergism of TNF-α and IFN-γ triggers inflammatory cell death, tissue damage, and mortality in SARS-CoV-2 infection and cytokine shock syndromes. Cell 184:149–168. https://doi.org/10.1016/j.cell.2020.11.025
51. Lenschow DJ, Lai C, Frias-Staheli N, Giannakopoulos NV, Lutz A, Wolff T, Osiak A, Levine B, Schmidt RE, García-Sastre A, Leib DA, Pekosz A, Knobeloch K-P, Horak I, Virgin HW. 2007. IFN-stimulated gene 15 functions as a critical antiviral molecule against influenza, herpes, and Sindbis viruses. Proc Natl Acad Sci U S A 104:1371–1376. https://doi.org/10.1073/pnas.0607038104
52. Keewan E, Beg S, Naser SA. 2021. Anti-TNF-α agents modulate SARS-CoV-2 receptors and increase the risk of infection through Notch-1 signaling. Front Immunol 12:641295. https://doi.org/10.3389/fimmu.2021.641295
53. Lee C-Y, Huang C-H, Rastegari E, Rengganaten V, Liu P-C, Tsai P-H, Chin Y-F, Wu J-R, Chiou S-H, Teng Y-C, Lee C-W, Liang Y, Chen A-Y, Hsu S-C, Hung Y-J, Sun J-R, Chien C-S, Chien Y. 2021. Tumor necrosis factor-alpha exacerbates viral entry in SARS-CoV2-infected iPSC-derived cardiomyocytes. Int J Mol Sci 22:9869. https://doi.org/10.3390/ijms22189869
54. Mohd Zawawi Z, Kalyanasundram J, Mohd Zain R, Thayan R, Basri DF, Yap WB. 2023. Prospective roles of tumor necrosis factor-alpha (TNF-α) in COVID-19: prognosis, therapeutic and management. Int J Mol Sci 24:6142. https://doi.org/10.3390/ijms24076142
55. Yuan L, Zhu H, Chen P, Zhou M, Ma J, Liu X, Wu K, Chen R, Liu Q, Yu H, Li L, Wang J, Zhang Y, Ge S, Yuan Q, Tang Q, Cheng T, Guan Y, Xia N. 2022. Infection, pathology and interferon treatment of the SARS-CoV-2 Omicron BA.1 variant in juvenile, adult and aged Syrian hamsters. Cell Mol Immunol 19:1392–1399. https://doi.org/10.1038/s41423-022-00923-9
56. Choi J-W, Kim J-W, Nguyen LP, Nguyen HC, Park E-M, Choi DH, Han KM, Kang SM, Tark D, Lim Y-S, Hwang SB. 2020. Nonstructural NS5A protein regulates LIM and SH3 domain protein 1 to promote hepatitis C virus propagation. Mol Cells 43:469–478. https://doi.org/10.14348/molcells.2020.0018
57. Reed LJ, Muench H. 1938. A simple method of estimating fifty per cent endpoints. Am J Epidemiol 27:493–497. https://doi.org/10.1093/oxfordjournals.aje.a118408
58. Khaitov M, Nikonova A, Shilovskiy I, Kozhikhova K, Kofiadi I, Vishnyakova L, Nikolskii A, Gattinger P, Kovchina V, Barvinskaia E, et al. 2021. Silencing of SARS - CoV - 2 with modified siRNA - peptide dendrimer formulation. Allergy 76:2840–2854. https://doi.org/10.1111/all.14850
59. Halgren T. 2007. New method for fast and accurate binding-site identification and analysis. Chem Biol Drug Des 69:146–148. https://doi.org/10.1111/j.1747-0285.2007.00483.x
60. Halgren TA. 2009. Identifying and characterizing binding sites and assessing druggability. J Chem Inf Model 49:377–389. https://doi.org/10.1021/ci800324m
61. Halgren TA, Murphy RB, Friesner RA, Beard HS, Frye LL, Pollard WT, Banks JL. 2004. Glide: a new approach for rapid, accurate docking and scoring. 2. Enrichment factors in database screening. J Med Chem 47:1750–1759. https://doi.org/10.1021/jm030644s